The characteristics and biological activity enhancements of melatonin encapsulations for skin care product applications

Phongsapak Phanphothong [a], Nattawadee Kanpipit [b], Suthasinee Thapphasaraphong [c],[*]

[a] *Pharmaceutical Chemistry and Natural Products Program, Faculty of Pharmaceutical Sciences, Khon Kaen University, Khon Kaen 40002, Thailand*
[b] *Faculty of Pharmaceutical Sciences, Khon Kaen University, Khon Kaen 40002, Thailand*
[c] *Department of Pharmaceutical Chemistry, Faculty of Pharmaceutical Sciences, Khon Kaen University, Khon Kaen 40002, Thailand*

ARTICLE INFO

ABSTRACT

Melatonin (MLT) exhibits antioxidant, ultraviolet protection, anti-inflammatory, and anti-aging properties. However, its effectiveness is limited by instability, a short half-life, and incompatible absorption. In this research, we encapsulated melatonin (MLT) in transfersomes (MT) and niosomes (MN) to enhance their properties and investigate their effects through in vitro cell assays using murine macrophages cells and human foreskin fibroblasts cells. The vesicle morphology, vesicle size, polydispersity index, zeta potential, entrapment efficiency (EE %), attenuated total reflectance-Fourier transform spectroscopy (ATR-FTIR) spectra, along with in vitro release, permeation profiles, and stability study were also evaluated. The results showed that both encapsulations displayed spherical morphology at the nanometric scale, their great physical stability and provided an EE% range of 58–78%. The MLT incorporation into the vesicle was confirmed by the ATR-FTIR spectra. Additionally, the encapsulation' release profiles fitted with the Higuchi model, indicating controlled release of melatonin. Furthermore, MT showed greater permeability than MN and MS including melatonin deposition. In cell assays, MT exhibited significantly higher nitric oxide inhibition and stimulation of collagen compared to MN and MS. Therefore, MT demonstrated the highest possibility for anti-inflammatory and collagen-stimulating activities that could be applied in pharmaceutical or anti-aging cosmetic products.

1. Introduction

Melatonin (*N*-acetyl-5-methoxy-tryptamine,) is a natural hormone produced and secreted from the pineal gland in brain and acts to control circadian rhythm and is involved in regulating the sleep system (Reiter et al., 2001). Melatonin can prevent DNA damage, oxidative stress, and apoptosis from ultraviolet radiation (UVR) irradiation in Human skin ex vivo (Skobowiat et al., 2018; Slominski et al., 2014) which cause skin anti-aging (Kleszczynski and Fischer, 2012). Melatonin has also been found to have beneficial effects on the skin which could regulate skin integrity in the human epidermal and dermal (Slominski et al., 2014). Moreover, there have been reports that melatonin could inhibit ultraviolet A (UVA)-induced matrix metalloproteinase-1 (MMP-1) and matrix metalloproteinase-3 (MMP-3) activation by suppressing lipid and protein oxidation (Koçtürk et al., 2019; Park et al., 2018), which affects collagen type I and type III in the dermis layer of skin. Melatonin suppressed the expression of ultraviolet B (UVB)-induced MMP-1 and related proteins (inflammatory proteins), increased procollagen, and

inhibited reactive oxygen species (ROS), MMP-1 and the hedgehog signaling pathway in human keratinocytes cell lines (HaCaT) (Park et al., 2018) including ultraviolet (UV) protection effects (Scheuer et al., 2014). Furthermore, melatonin has anti-inflammatory via reducing (iNOS) nitric oxide synthase expression and (NO) nitric oxide inhibition (Kang et al., 2013; Phiphatwatcharaded et al., 2014; Sangchart et al., 2021). Therefore, melatonin has anti-inflammatory and antioxidant capabilities to prevent mitochondrial damage, DNA damage, oxidative stress from external environmental variables which generate anti-aging effects (Bocheva et al., 2022). These melatonin properties are applicable to develop as anti-aging, anti-wrinkle, and anti-inflammatory skin care products.

However, melatonin is sensitive to environmental factors such as light, temperature, and moisture, thus encapsulation of melatonin is an alternative way to be applied as a skin care product. One type of encapsulation, a lipid-based drug delivery system, such as transfersomes and niosomes could help to protect the active compounds from environmental factors such as oxidation, light, humidity, heat, and acidity

(Casanova and Santos, 2016) including controlled drug delivery improvement, enhancement of permeation, reduction of toxicity and side effects. Melatonin loaded elastic liposomes developed for transdermal delivery was found to enhance permeation of the formulation to deeper layers of the skin (Dubey et al., 2006). Melatonin entrapped niosome was developed as a niosomal gel could provide a tool to sustain systemic melatonin absorption and prolong anti-inflammatory activity (Netweera et al., 2013; Priprem et al., 2014). In addition, transmucosal melatonin entrapped niosome was developed to improve absorption and prolonged systemic circulation (Priprem et al., 2018).

Transfersomes are more deformable and flexible than liposomes, which allows them to pass through the pores of the skin more easily. Transfersomes have several desirable properties for topical application, such as elasticity and flexibility, and these properties are affected by the nature of the edge activator (as Tween 20, 60, 80, etc.) and phosphatidylcholine components (Fernández-García et al., 2020). Transfersomes have provided controlled release of therapeutic agents, enhance skin permeation (Opatha et al., 2020) and become interesting for transdermal drug delivery due to their ultra-deformability while passing through the skin (Rai et al., 2017). In addition, transfersomes were found to protect the active compounds from undesired photodegradation (Demartis et al., 2021).

In this study, we compared melatonin entrapped in transfersomes (MT) and niosomes (MN) with free melatonin solution (MS) for their characteristics such as appearance, size, polydispersity index (PDI), zeta potential, percent entrapment efficiency (%EE), and attenuated total reflectance - Fourier transform spectroscopy (ATR-FTIR) including melatonin release and permeation. Furthermore, the biological activities in cell assays such as cytotoxicity, nitric oxide inhibition, and collagen production were investigated on murine macrophages cells (RAW 264.7) and human foreskin fibroblasts cells (HFF-1). The results could provide the potential formulation for anti-inflammatory and collagen synthesis activities which can be applied as a skin anti-aging product.

2. Materials and methods

2.1. Materials

Phosphatidylcholine 90% (PC) was purchased from Myskinrecipes (Bangkok, Thailand), Tween 80 was purchased from Chem-Supply (Gillman, SA, Australia), Melatonin was purchased from Purebulk (Roseburg, OR, USA), and PEG 400 were purchased from Sigma Aldrich (St. Louis, MO, USA), acetonitrile (ACN) was purchased from Merck KGaA (Darmstadt, Germany), disodium hydrogen orthophosphate, and sodium dihydrogen orthophosphate, were purchased from Ajax Finechem (Taren Point, NSW, Australia) all chemicals used in this study were AR grade.

2.2. Methodology

2.2.1. Melatonin entrapment preparation

The lipid-based nanoparticle was prepared to entrap melatonin by sonication method (Bansal et al., 2013; Kim et al., 2004). The melatonin entrapped transfersomes (MT) were prepared from a mixture of 85.36 mg of phosphatidyl choline (PC), 13.1 mg of Tween 80 and 50 mg of melatonin in 500 µL of PEG 400 and adjusted to 10 mL with phosphate buffer pH 7.4 (Agrawal et al., 2015; Chen et al., 2020). The final concentrations of PC and Tween 80 were 11 mM and 1 mM, respectively. The final concentration of melatonin was 0.5% w/v. After that, the mixture was vortexed for 5 min by a vortex mixer (Biosan V-1 plus, Riga, Latvia), and sonicated for 30 min by using a low-frequency ultrasonic bath (CREST 230 T, NY, USA). Whereas melatonin entrapped niosomes (MN) were prepared from a mixture of 3.9 mg of cholesterol (CL) and 4.3 mg of Span 60 in 5 mL of phosphate buffer pH 7.4 and then the mixture was heated at 60 °C for 10 min. Then, 50 mg of melatonin dissolved in 500 µL of PEG 400 was added and adjusted to 10 mL with

phosphate buffer pH 7.4. The final concentrations of CL and Span 60 were 1 mM. The final concentration of melatonin formulation was 0.5% w/v. The suspension was vortexed for 5 min and sonicated for 30 min by the low-frequency ultrasonic bath.

2.2.2. Vesicle characteristic evaluation

The vesicle characterization was determined for measurement of size, polydispersity index (PDI), and zeta potential by dynamic light scattering (DLS) using a Zeta Sizer Nano ZS (Malvern Instruments Ltd., Malvern, U.K.) (Caddeo et al., 2018).

2.2.3. Morphology of vesicles

The morphology of vesicles was evaluated by transmission electron microscopy (TEM, FEI, TECNAI G^2, Netherlands). The samples were diluted 50-fold with phosphate buffer pH 7.4, dropped onto carbon-coated copper grids. After samples were air-dried at room temperature (normal conditions) were observed under TEM (Kuznetsova et al., 2022).

2.2.4. Entrapment efficiency (%EE)

The entrapment efficiency of vesicles was performed using Vivaspin® 2, MWCO 30 KDa (Sartorius AG, Göttingen, Germany). A 1 mL sample was centrifuged for 30 min at 5000 x G by centrifuge (Kubota 6200, Tokyo, Japan) to separate the melatonin contained transfersome or niosome vesicles from unentrapped melatonin (Gao et al., 2021). The amount of melatonin in the vesicle was extracted using Phosphate buffer pH 7.4 with 25% propylene glycol (PG) and 25% ethanol (EtOH) by 1:1 ratio with samples. The amount of melatonin in the vesicle and unentrapped melatonin parts were measured by using a fluorescence microplate reader, FMR (EnSight® multimode microplate reader with a fluorescence detector, PerkinElmer, Waltham, MA, USA) at the excitation wavelength of 274 nm and the emission wavelength of 370 nm. The fluorescence microplate reader for melatonin determination was validated compared to standard HPLC method are shown in supporting information (Table S13 and Fig. S7-S10). The %EE was calculated according to Eq. (1) (Priprem et al., 2018).

$$\%EE = \frac{amount\ of\ MLT\ in\ vesicle}{amount\ of\ MLT\ in\ vesicle + amount\ of\ untrapped\ MLT} \times 100$$

(1)

2.2.5. Stability test

The stability test used a heating-cooling cycle test. The formulation was tested under conditions switching low-temperature (4 °C) to high-temperature (45 °C), which performed storage conditions between 4 °C for 24 h and 45 °C for 24 h (1 cycle) conducted of 6 cycles. Then the size, zeta potential, PDI, and %EE were determined before and after storage condition. This method was modified as previously described (Estanqueiro et al., 2014; Fitrya et al., 2022).

2.2.6. Attenuated total reflectance (ATR) - fourier transform spectroscopy (FTIR)

The ATR-FTIR spectra were used to study the chemical interaction between melatonin and vesicles, which was measured by the FTIR spectrometer Bruker tensor II series (Billerica, MA, USA). The aqueous samples of blank transfersomes (BT), blank niosomes (BN), melatonin-loaded transfersomes (MT) and melatonin loaded-niosomes (MN) were pipetted 5 µL and dropped on the crystal surface of the machine. Then an air dryer (cold air) was used to dry the samples for 10 min. An analyzation was performed at the spectral range 4000–400 cm^{-1}, resolution 4 cm^{-1} for 64 co-added scans per spectrum.

2.2.7. In vitro release study

The in vitro release of melatonin from MT, MN and 0.5% MLT solution in phosphate buffer pH 7.4 with 5% PEG 400 (MS) were investigated using a Franz diffusion cell method (Franz, 1975). The cellulose

dialysis membrane (CelluSep®, T4, MWCO 12–14 kDa, Membrane Filtration Products, TX, USA) was rinsed in warm distilled water for 30 min to remove preservative and soaked overnight in a medium (Attia et al., 2007; Panwar et al., 2010). Next, the membrane was washed with warm distilled water and medium and placed between the donor and receptor compartments. The receptor chamber was filled with 5 mL of 25% propylene glycol (PG) and 25% EtOH in phosphate buffer pH 7.4 (Farah et al., 2019; Haq and Michniak-Kohn, 2018). The Franz diffusion cell was placed on the multi position magnetic stirrer (VELP Scientifica Multistirrer Digital 6, Usmate Velate (MB), Italy) and stirred at 800 rpm. A circulating bath (LAUDA Alpha A6, Königshofen, Germany) was used to maintain the medium temperature at 37 ± 0.1 °C. Then the donor chamber was filled with 1 mL of sample and covered with parafilm and aluminum foil. The receptor medium was withdrawn (0.6 mL) at set time intervals (0.5, 1, 2, 4, 6, 8, 12, 24 h) and immediately replaced with an equal volume of fresh medium. The melatonin content was determined by a fluorescence microplate reader.

2.2.8. Release kinetics

The data of release kinetics according to four models, zero-order (cumulative release percentage versus time), first-order (log cumulative drug release percentage versus time), and Higuchi model (cumulative drug release percentage versus square root of time) were investigated (Higuchi, 1963). The correlation coefficients for all the release kinetics calculated using linear regression analysis. The Korsmeyer-Peppas model (log cumulative drug release percentage versus log time) was used to analyze the mechanism of drug release and the diffusion kinetics in which the n exponent was obtained from the slope of linear regression. Whereas n is releasing exponent indicative of the release mechanism, if $n < 0.5$, a Fickian diffusion mediated drug release occurs while if $0.5 < n < 1$, a non-Fickian transport is predominant, $n = 1$ to Case II (relaxational) transport and $n > 1$ to super case II transport (Korsmeyer et al., 1983).

2.2.9. In vitro permeation study

The in vitro skin permeation study was carried out by a modified Franz diffusion cell using Strat-M® membrane (Merck KGaA, Darmstadt, Germany). The method was performed in a similar manner as same as drug release study and the receptor chamber was filled with phosphate buffer pH 7.4 (Zsikó et al., 2019). The graph between %cumulative amount and time was constructed. The cumulative permeation steady-state flux (J_{SS}) was obtained from the slope of linear regression graph. The lag time (T/lag) was calculated by extrapolating the cumulative amount permeated profile's linear area to the x-axis intercept. The other parameters, permeability coefficient (P), including enhancement ratio (ER), were calculated according to Eq. (2). Whereas MS was used as a control.

$$P = J_{SS}/C_0 \text{(Initial concentration)}$$
$$ER = J_{SS} \text{ test}/J_{SS} \text{ control} \tag{2}$$

A skin deposition study was used for the evaluated amount of melatonin accumulation in the Strat M® membrane of various formulations. After 24 h of permeation study, the Strat M® membranes were removed from the Franz diffusion and extracted for melatonin. The membranes were placed in a centrifuge tube of 50 mL containing 5 mL of (25% propylene glycol (PG) and 25% EtOH in phosphate buffer pH 7.4) and sonicated for 1 h (Al-mahallawi et al., 2019; Ameri et al., 2018). After that, the amount of melatonin was determined for fluorescence intensity by a fluorescence microplate reader.

2.2.10. Cell culture assay

Human foreskin fibroblast cells (HFF-1 cells) were purchased from ATCC (SCRC-1041, USA). and murine macrophage cell line (RAW 264.7 cells) was obtained from Dr. Pramote Mahakunakorn (Faculty of Pharmaceutical Sciences, Khon Kaen University, Khon Kaen Thailand). Cells were cultured in 75 cm²-flasks in complete medium (DMEM high

glucose supplement, with 10% Fetal bovine serum (FBS), 100 µg/L streptomycin, and 100 IU/mL penicillin). The cells were maintained and incubated at 37 °C with 5% CO_2.

2.2.10.1. Cell viability assay.
Human foreskin fibroblast cells (HFF-1 cells) or murine macrophage cells (RAW 264.7 cells) were seeded into 96 well plates at an initial concentration of 1.5×10^4 cells/well in 100 µL of culture medium and incubated for 24 h at 37 °C with 5% CO_2. Then the medium was removed after 24 h. The cells were treated with 100 µL of samples such as MT, MN, MS, BT or BN in culture media (1:10 ratio). After incubation for 24 h, at 37 °C with 5% CO_2, the medium was removed and 100 µL of MTT ([3(4,5-dimethyl thiazolyl-2)-2,5-diphenyltetrazolium bromide]) 0.5 mg/mL was added to each well and then incubated for 3 h at 37 °C with 5% CO_2. Lastly, the crystals of formazan in each well were dissolved by dimethyl sulfoxide (DMSO) 100 µL. The absorbance of the mixture was measured at 570 nm using a microplate reader and calculated for cell viability (Chiong et al., 2013). The media from non-treated cells was a negative control (control). The experiment was executed with three replicates, and the % cell viability was calculated as the following Eq. (3).

$$\%\text{Cell viability} = \frac{\text{absorbancesample}}{\text{absorbancecontrol}} X 100 \tag{3}$$

2.2.10.2. Nitric oxide inhibition assay.
RAW 264.7 cells were seeded in 96 well plates at a density of 1.5×10^4 cells/well with culture medium and incubated for 24 h at 37 °C with 5% CO_2. Then, the media was aspirated and replaced by MT, MN, MS or 200 µM N_ω-Nitro-L-arginine methyl ester hydrochloride (L-NAME, positive control) in culture media (1:10 ratio) with of 1 µg/mL lipopolysaccharide (LPS) to give a total volume of 100 µL and incubated for 24 h at 37 °C with 5% CO_2 (Chiong et al., 2013; Dzoyem et al., 2016). LPS was used to induce nitric oxide production. Then, the 100 µL/well supernatants were transferred into new 96 well plates. Griess reagent (1% sulfanilamide in 5% phosphoric acid and 0.1% N-(1 -Naphthyl) ethylenediamine in DI water) was added (100 µL/well) and incubated for 30 min (in the dark at room temperature). The absorbance was measured at 540 nm using a microplate reader. The media with LPS from non-treated cells was used as a control (control). The media without LPS from non-treated cells was a negative control ((−)control)). Nitric oxide (NO) inhibition was performed with three replicates and was calculated per Eq. (4) (Tewtrakul and Itharat, 2007).

$$\%\text{NO inhibition} = \frac{\text{absorbancecontrol–absorbancesample}}{\text{absorbancecontrol–absorbance}(-)\text{control}} X 100 \tag{4}$$

2.2.10.3. Picrosirius red assay.
The collagen determination using picrosirius red assay method was modified from Taskiran et al. (Taşkiran et al., 1999). In brief, 100 µL of each sample (media from HFF-1 cells) was mixed with 100 µL of 0.5 M acetic acid and 1 mL of dye solution reagent (Direct red 0.00067 g/mL in picric acid), then sonicated for 30 min. The mixture was centrifuged at 12,000 rpm for 10 min. The supernatant was removed. The precipitate was added to 1 mL of 0.1 M HCl and then centrifuged at 12,000 rpm for 10 min. The mixture was dissolved by 1 mL of 0.5 N NaOH. The absorbance of the sample was measured at 540 nm. The collagen content was calculated and compared with the calibration curve of standard collagen type I (Longsri et al., 2021).

2.2.11. Statical analysis

Data are presented as mean ± standard error of mean (SEM) with three replications ($n = 3$) and were analyzed using SPSS version 28 (licensed KKU software). Differences between groups were assessed by one-way analysis of variance (ANOVA) by Tukey's test. The comparison in stability test was evaluated by Paired sample *t*-test. A *p*-value of <0.05 was considered statistically significant.

3. Results and discussion

3.1. Vesicle characteristic evaluation

3.1.1. Particle size, Polydispersity Index (PDI), Zeta potential

MT, MN, BT and BN were prepared and evaluated for their physical properties such as particle size, PDI and zeta potential (Table 1). The mean intensity diameter of BT and BN were 272.00 ± 3.46 and 337.70 ± 44.61 nm, respectively. Whereas the mean intensity diameter of MT and MN were 119.57 ± 12.15 nm and 163.97 ± 25.05 nm, respectively, showing no significant difference. Though, MT and MN demonstrated significantly smaller particle sizes compared to BT and BN ($p < 0.05$). This reduction in size can be attributed to melatonin's interaction with the lipid bilayer, which resulted in increased membrane fluidity and a decrease in the thickness of the lipid bilayer. (De Lima et al., 2007; Dies et al., 2015; Hou et al., 2022). The PDI index values for all samples were <1 (ranging from 0.33 ± 0.04 to 0.89 ± 0.04), suggesting a uniform particle size distribution. In addition, the zeta potential of all vesicles was less than -30 mV (Table 1), indicating excellent physical stability of the vesicles.

3.1.2. Entrapment efficiency (%EE)

The percentage entrapment efficiency (%EE) was evaluated to estimate the capability of the vesicles to entrap melatonin. The %EE of MT (74.95 ± 0.81) showed significantly higher ($P < 0.05$) compared to MN (58.52 ± 1.80). The results are shown in Table 1. The utilization of long carbon chain surfactants, such as C16 and C18, has been shown to enhance lipophilicity and improve the entrapment of the drug (Caddeo et al., 2018). Moreover, higher lipid content in transfersomes has been found to increase the entrapment efficiency of MLT (Alvi et al., 2011). Similarly, the type of surfactant, the amount of cholesterol and the quantity of incorporated drug can influence the entrapment efficiency of niosomes (Balakrishnan et al., 2009).

3.1.3. Stability test

The stability test was performed by the heating-cooling cycle test conducted of 6 cycles, and the results are shown in Fig. 1. The particle size, PDI, zeta potential, and %EE of MT exhibited no significant differences between the before and after storage conditions. Whereas, the particle size, PDI, and zeta potential of MN exhibited significant differences between the before and after storage conditions, except for the % EE.

During the stability study, a decrease in the particle size of MN was observed after storage. This reduction in particle size may be attributed to the impact of elevated temperatures experienced during the storage period. The increased temperature likely induced changes within the system by promoting the fluidization of the bilayer and diminishing the electrostatic repulsive forces generated by the lipid bilayer's head. Furthermore, %EE for both MT and MN showed no significant difference

after storage condition. The encapsulation of MLT in nanoparticles serves to protect it from degradation, leading to an increase in %EE after the stability test (Mao et al., 2019). However, MT offers enhanced physical stability compared to MN when preparing MLT encapsulations using the sonication method.

3.1.4. Morphology of transfersomes and niosomes

The transmission electron microscope (TEM) images revealed that both MT and MN exhibited spherical shapes, with particle diameters ranging from 100 to 200 nm (Fig. 2). These images confirmed the successful formation of transfersome and niosome vesicles which showed the spherical shape as well as the previous researches (Fitrya et al., 2022; Uthaiwat et al., 2021).

3.1.5. ATR-FTIR characterization

The FTIR spectra of compositions in transfersomes are shown in Fig. 3. Phosphatidylcholine (PC) (Fig. 3A) provided the peaks at 2923 cm^{-1} and 2853 cm^{-1} of the acyl chain in CH$_3$ and CH$_2$ stretching, including 1465 cm^{-1} of CH$_2$ bending scissoring, 1736 cm^{-1} of C=O stretching bands of the polar group of PC, 1064 cm^{-1} of P-O-C stretching, 1245 cm^{-1} and 968 cm^{-1} of PO$_2$ and $^+$N(CH$_3$)$_3$ antisymmetric stretching (Park et al., 2021; Terakosolphan et al., 2018). PEG 400 (Fig. 3B) showed the peak at 3449 cm^{-1} of O—H stretching, 2865 cm^{-1} CH$_2$ stretching, 1454 cm^{-1} of C—H bending, 1249 cm^{-1} of C—O stretching and 1095 cm^{-1} of C-O-C stretching (Marcos et al., 2017; Sahu et al., 2022). Tween 80 (Fig. 3C) were observed the peaks at 3492 cm^{-1} of O—H stretching, 2857 cm^{-1} of CH$_2$ stretching of an alkyl chain, 1736 cm^{-1} of C=O stretching, 1458 cm^{-1} of C—H bending scissoring of an alkyl chain and 1095 cm^{-1} of C-O-C stretching (Kura et al., 2014; Sahu et al., 2022). Melatonin (Fig. 3D) showed the peaks at 3275 cm^{-1} of N—H stretching, 1618 cm^{-1} of amide I C=O stretching, 1552 cm^{-1} of amide II C—N stretching and 1210 cm^{-1} of C—N stretching (Parvez et al., 2021; Uthaiwat et al., 2021).

The FTIR spectrum of BT (Fig. 3E) provided the band at 3385 cm^{-1} of O—H stretching and the peaks at 2868 cm^{-1} of CH$_2$ stretching, 1734 cm^{-1} and 1646 cm^{-1} of C=O stretching, 1457 cm^{-1} of CH$_2$ bending scissoring, 1248 cm^{-1} of PO$_2$ stretching and 1091 cm^{-1} of P-O-C and C-O-C stretching. Comparison to BT, FTIR spectrum of MT (Fig. 4F) provided the additional peaks at 1558 cm^{-1} of amide II C—N stretching and 1219 cm^{-1} of amide III C—N stretching of entrapped MLT which were shifted from 1552 cm^{-1} of amide II C—N stretching and 1210 cm^{-1} of C—N stretching of free MLT suggesting MLT was entrapped in the phospholipid bilayer (Parvez et al., 2021). The peaks at 3357 cm^{-1} of O—H stretching and 1653 cm^{-1} of C=O stretching from MT were shifted from 3385 cm^{-1} (O—H stretching) and 1646 cm^{-1} (C=O stretching) of BT and the peak at 1734 cm^{-1} was not observed in MT. Hence, the shifted peaks could confirm the interaction between amide functional group of MLT and the OH group of transfersome (Hasibi et al., 2020). Additionally, these shifts can be attributed to interaction with the polar region of a phospholipid bilayer in FTIR spectrum of MT (Sahin et al., 2013).

The FTIR spectra of composition in niosomes are shown in Fig. 4. FTIR spectrum of cholesterol (Fig. 4A) provided the peak at 2930 cm^{-1} and 2866 cm^{-1} of CH$_3$-CH$_2$ stretching, C—H bending, 1054 cm^{-1} of C—O stretching and 799.4 cm^{-1} of C—H methylene rocking (Akbari et al., 2022; Farmoudeh et al., 2020). Span 60 (Fig. 4B) showed the peaks at 3375 cm^{-1} of O—H stretching. 2916 cm^{-1} and 2849 cm^{-1} of CH$_3$-CH$_2$ stretching, 1734 cm^{-1} of C=O stretching, 1174 cm^{-1} of C-O-C stretching, and 721 cm^{-1} of CH$_2$ rocking (Farmoudeh et al., 2020). PEG 400 (Fig. 4C) and melatonin (Fig. 4D) showed the peaks as same as in Fig. 3D.

The FTIR spectrum of BN (Fig. 4E) provided the band at 3386 cm^{-1} of O—H stretching, 2867 cm^{-1} of CH$_2$ stretching, 1644 cm^{-1} of C=O stretching, 1455 cm^{-1} of CH$_2$ bending scissoring, 1091 cm^{-1} of C-O-C stretching, suggesting interaction with the polar region of the lipid bilayer by increasing hydrogen bonding (Terakosolphan et al., 2018).
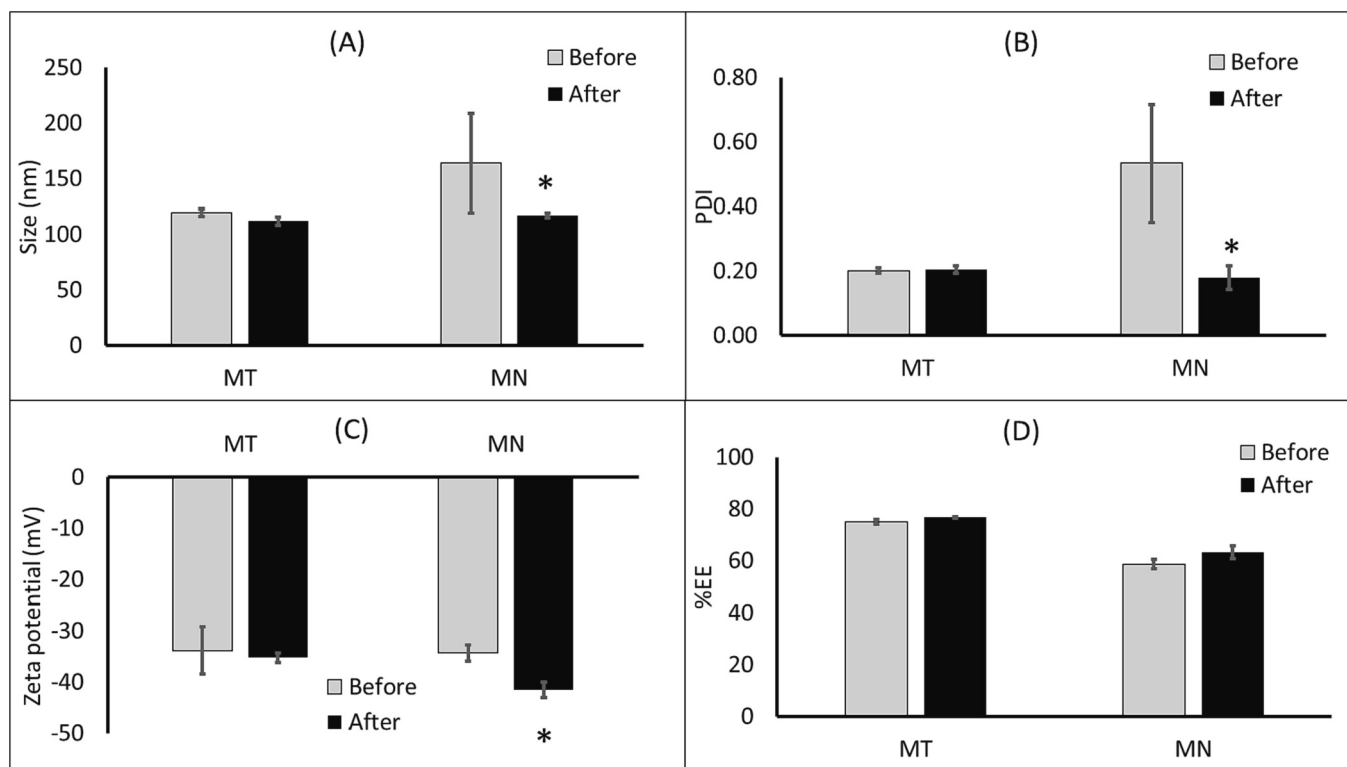
Table 1
SIZE, PDI, Zeta potential, and %EE, including Stability test of the formulation. All the values are shown as mean $\pm$ SEM ($n = 3$).

Formulation	Size (nm)	PDI	Zeta potential (mV)	%EE
BT	272.00 ± 3.46^b	0.33 ± 0.04^a	-46.27 ± 3.18^a	–
MT	119.57 ± 12.15^a	0.20 ± 0.01^a	-33.80 ± 4.57^b	74.95 ± 0.8^b
BN	337.70 ± 44.61^c	0.89 ± 0.04^c	$-41.17 \pm 6.95^{a,b}$	–
MN	163.97 ± 25.05^a	0.53 ± 0.18^b	-34.30 ± 1.57^b	58.52 ± 1.80^a

BT: Blank transfersomes. MT: MLT-loaded transfersomes. BN: Blank niosomes. MN: MLT-loaded niosomes.
[a-c] letters indicate difference significance between the group at p < 0.05.

Fig. 1. Stability test of MLT-loaded transfersomes (MT) and MLT-loaded niosomes (MN): SIZE, PDI, Zeta potential, and %EE of MT and MN before and after storage condition. All the values are shown as mean ± SEM (n = 3). * indicates a significant difference between before and after storage condition of each groups ($p < 0.05$).
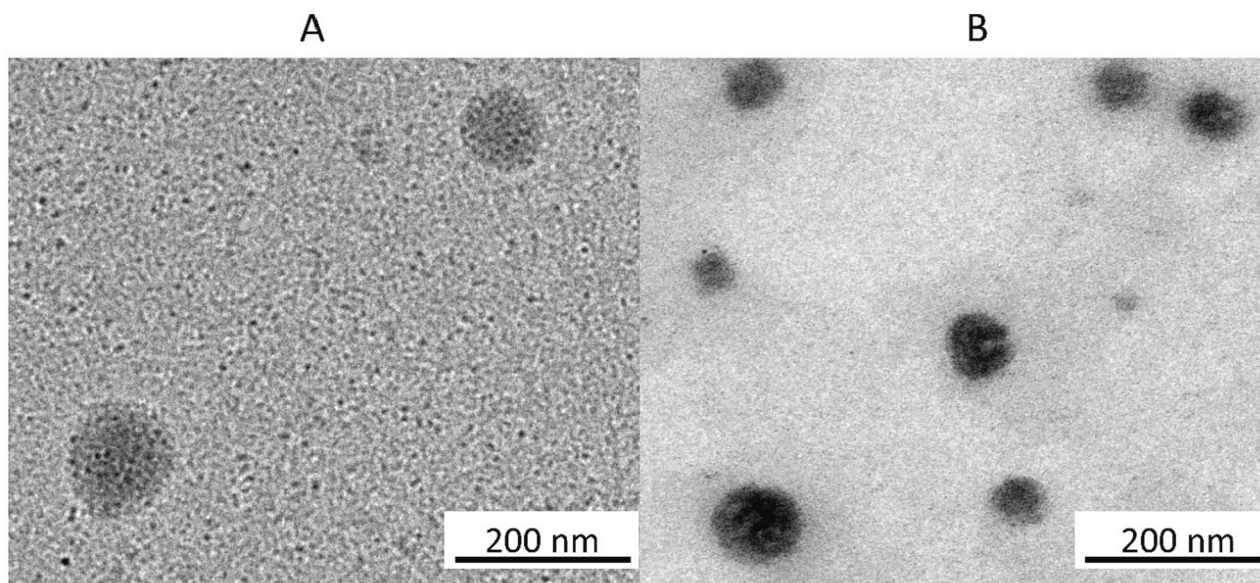

Fig. 2. Transmission electron microscope (TEM) images of (A) MLT-loaded transfersomes (MT); (B) MLT-loaded niosomes (MN).

The FTIR spectrum of MN (Fig. 4F) offered the additional peak at 1558 cm^{-1} of entrapped MLT (amide II C—N stretching) which was shifted from 1552 cm^{-1} of free MLT demonstrated interaction of MLT with the lipid bilayer of niosomes. Furthermore, the peak at 1653 cm^{-1} of C=O stretching which was shifted from 1644 cm^{-1} of BN[1] which attributed interaction with the polar region of the lipid bilayer of niosomes (Sahin et al., 2013). The shifted peaks could confirm the interaction between amide group of MLT and OH group of span 60 in niosome (Kumar and Rajeshwarrao, 2011).

The earlier research on MLT-loaded liposomes revealed that MLT

might insert between phosphatidylcholine molecules in the membrane, causing a reorganization of the lipid molecules (De Lima et al., 2007). Like liposomes, MLT was observed to be inserted between the phosphatidylcholine molecules and surfactants in MT as well as MN (Fig. 5). Consequently, this interaction between phospholipids and surfactants within transfersomes could enhance the fluidity of the bilayer.

3.1.6. In vitro release

The in vitro release of melatonin from MT and MN was analyzed by Franz diffusion cell using a cellulose membrane compared to melatonin
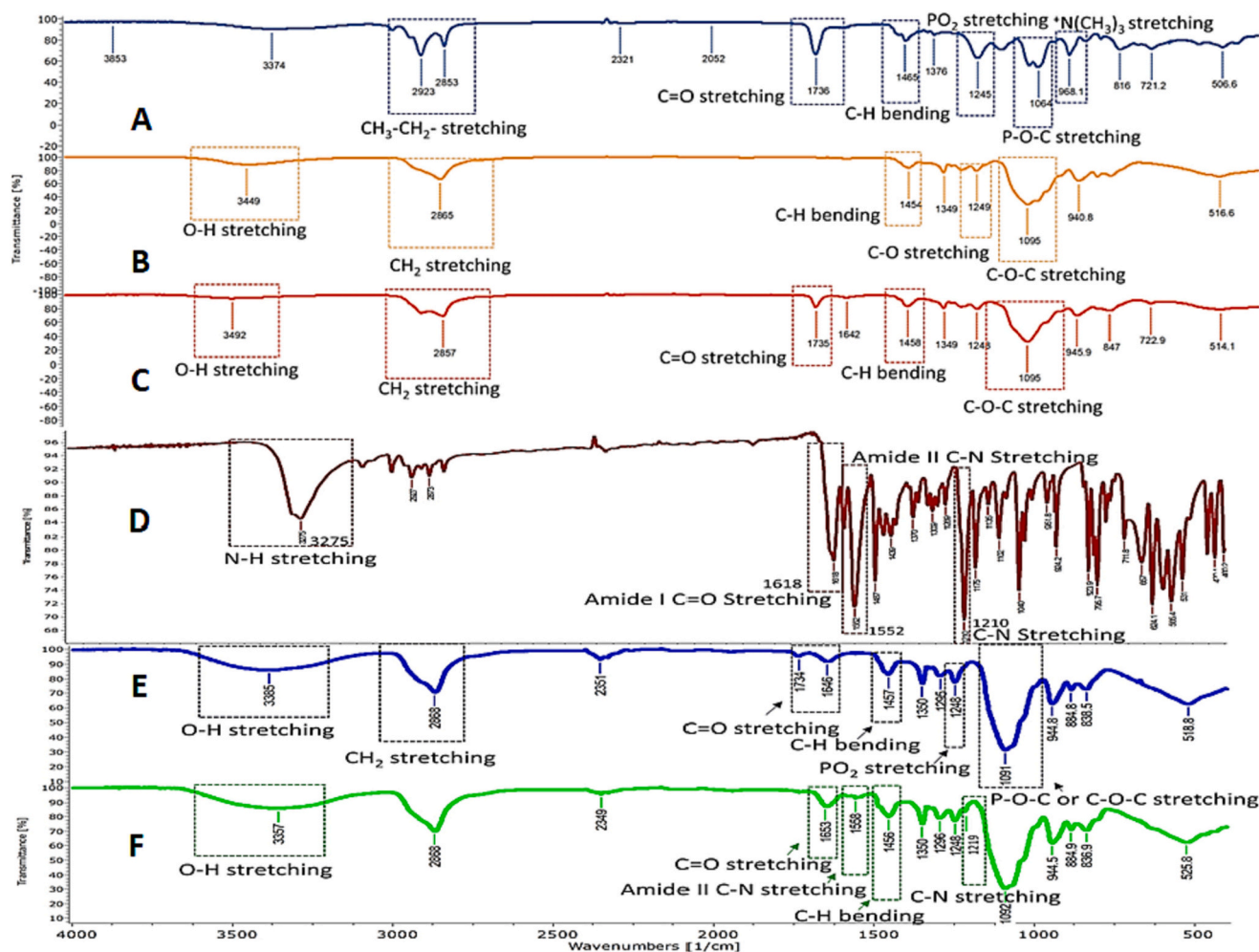
Fig. 3. FTIR spectra of transfersomes: (A) Phosphatidylcholine (PC), (B) PEG 400, (C) Tween 80 (D) Melatonin (MLT), (E) Blank transfersomes (BT), and (F) MLT-loaded transfersomes (MT).

solution (MS). The result showed that the highest cumulative release of MT was $74.79 \pm 3.99\%$ at 24 h and the highest cumulative release of MN was $66.84 \pm 0.24\%$ at 24 h (Fig. 6). Whereas the cumulative release of MS demonstrated the highest release rate to $102.28 \pm 1.85\%$ at 8 h. Therefore, MLT-loaded transfereome and niosome formulations achieved the desired delayed release profile for melatonin (Fig. 6).

In case of MT, the association of surfactant molecules with the lipid bilayer resulted in an enhanced drug partitioning and increased drug release from the vesicles (Marwah et al., 2016). Whereas MN demonstrated lower membrane permeability compared to MT. The presence of cholesterol in MN is responsible for the increased vesicle membrane rigidity and decreased fluidity observed. These changes in membrane properties can impede the release of drugs through the vesicle membrane, ultimately leading to a decrease in drug release (Auda et al., 2016; Shah et al., 2020).

3.1.7. Release kinetics models

Several models were evaluated to predict MLT release kinetics of MT, MN and MS (Table 2). It was established that the Higuchi kinetic equation provided the best fit for the release profiles of MT, MN and MS (Fig. S3-S5), with R^2 values of 0.9955, 0.9551 and 0.8287, respectively. These findings implied that they exhibited traits consistent with a controlled release system, as observed in a prior investigation (Moroni and Garcia-Bennett, 2021). The n is a parameter from the Korsmeyer-Peppas model that describes the mechanism of drug release MT formulation exhibited n at 0.6870 whereas MS exhibited n at 0.7143.

Both MT and MS provided n in the range of $0.5 < n < 1.0$ (Table 2) which indicated a non-Fickian anomalous release of MLT, primarily driven by diffusion and matrix deterioration (Kateh Shamshiri et al., 2019). Whereas the n value of MN was 0.3766 which indicates $n \leq 0.5$ as well as the previous research of caffeine from niosomal formulations (Khazaeli et al., 2007). This result suggested that MLT release from niosomes follows Fickian diffusion driven by a chemical potential gradient (Dabbagh Moghaddam et al., 2021). These outcomes demonstrated that the MLT-loaded transfereome and niosome formulations achieved the anticipated delayed release profile for melatonin.

3.1.8. In vitro permeation

Fig. 7 illustrates the in vitro permeation profiles of MS, MT, and MN, while Table 3 presents the corresponding permeability parameters for these formulations. MT exhibited significantly higher values for Flux (40.74 ± 0.33 µg/cm^2.h), cumulative amount permeated at 24 h (Q24, 858.44 ± 8.08 µg/cm^2), enhancement ratio (ER, 8.7), permeability coefficient (P, $8.15 \pm 0.07 \times 10^{-3}$ cm^2/h) and Lag time (T$_{lag}$) compared to MS and MN (Table 3). Furthermore, MT exhibited significantly higher skin deposition of MLT (392.47 ± 6.83 µg/cm^2) compared to MN (214.49 ± 8.90 µg/cm^2) and MS (270.28 ± 4.46 µg/cm^2).

Tween 80, a non-bulky carbon chain, was found to provide high flexibility to transfersomes, which provided elastic deformability (El Zaafarany et al., 2010). Therefore, transfersomes can deform through the gap between corneocytes and reform after passing through the stratum corneum (Alvi et al., 2011; Avadhani et al., 2017; Demartis
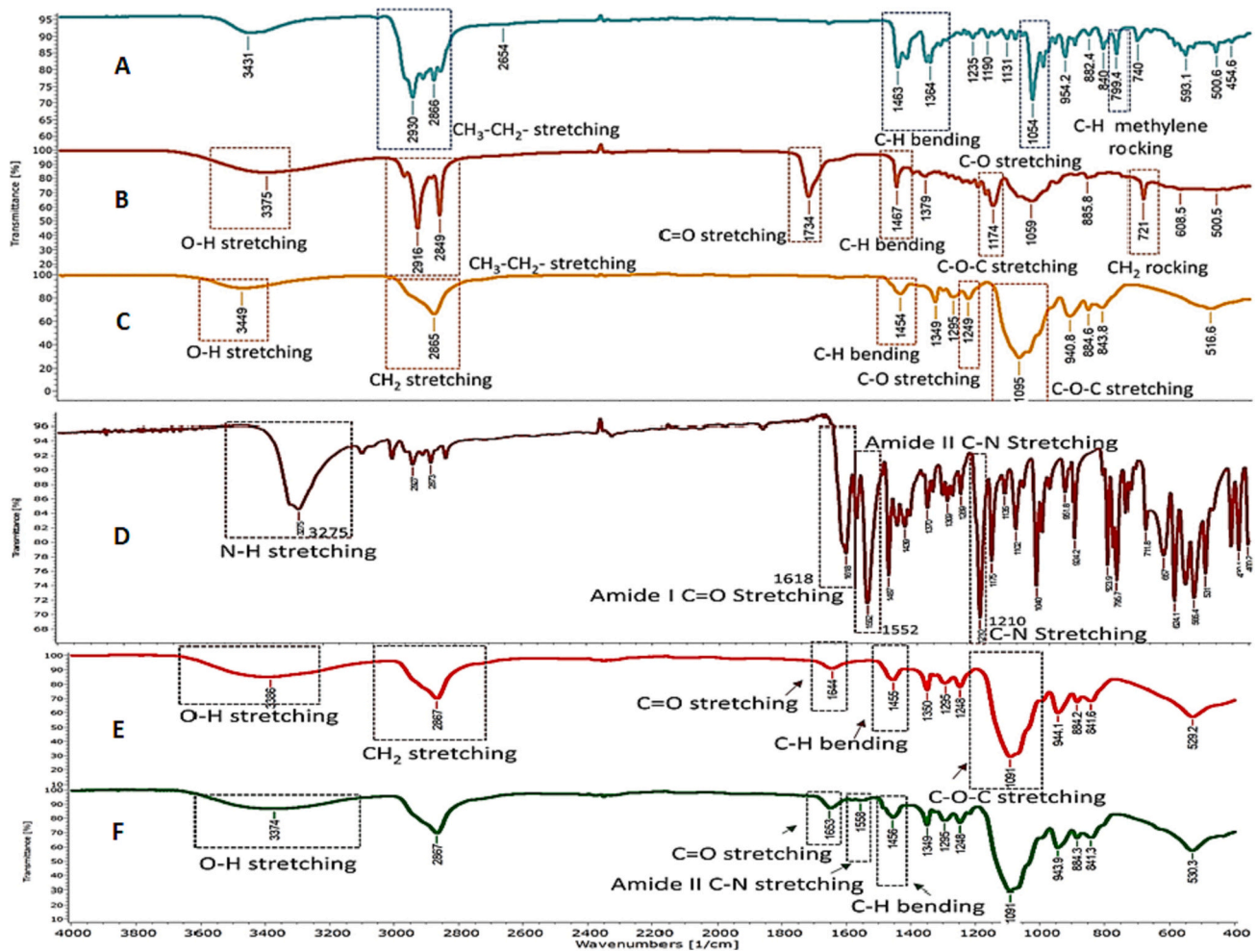
Fig. 4. FTIR of niosomes: (A) Cholesterol, (B) Span 60, (C) PEG 400 and (D) Melatonin (MLT), (E) Blank niosomes (BN), and (F) MLT-loaded niosomes (MN).

et al., 2021; Gupta et al., 2005). Moreover, transfersomes have shown an ability to permeate under non-occlusion conditions, which is required to initiate a transepidermal osmotic gradient across the skin (Opatha et al., 2020). A previous study has indicated that transfersomes exhibit higher elasticity and penetration capabilities compared to niosomes. Furthermore, the inclusion of lipids in the nanovesicles facilitated the generation and maintenance of the necessary physicochemical conditions of the skin, resulting in improved permeation and retention (Alvi et al., 2011; Gupta et al., 2005).

To reduce animal experimentation and expedite drug research, initial screening can be performed using skin artificial membranes (Strat ®M membrane). However the final product testing should be conducted using human skin to obtain accurate permeation data and provides a more reliable assessment of the product's interaction with human skin (Neupane et al., 2020).

3.1.9. Cell assays

3.1.9.1. Cell viability. Most of the samples exhibited no toxicity, as evidenced by cell viability exceeding 80%, in both RAW 264.7 cells (Fig. 8A) and HFF-1 cells (Fig. 9A). However, the effects of MS on RAW 264.7 cells and BN on HFF-1 cells showed cell viability lower than 80% and. Interestingly, the cell viability of MS exhibited no significant difference compared to the control and MN in Raw 264.7 cells while, the cell viability of MS showed no significant difference compared to BT, BN, and MN in HFF-1 cells. However, the previous research demonstrated that transfersomes were more effective in increasing cell viability

compared to agents without transfersomes (Wu et al., 2019).

3.1.9.2. NO inhibition. Nitric oxide inhibition testing was performed using LPS-stimulated RAW 264.7 cells and Griess reagent to determine nitric oxide levels. The results are shown in Fig. 8B. There was no significant difference observed in the nitric oxide inhibition between MT (82.10%) and MS (84.73%). While MN showed an inhibition of 76.13%. This indicates that MS and MT exhibited a more potent inhibitory effect on nitric oxide compared to MN. However, all samples treatment showed lower levels of nitric oxide production inhibition than the positive control, L-NAME (90.45%). In this study, MT showed the highest inhibitory effect against nitric oxide production in RAW 264.7 cells due to the higher entrapment efficiency, permeated Flux, and MLT release than MN. Whereas free MLT (MS) produced the most toxicity among all samples.

The molecular pathway that induces inducible nitric oxide synthase (iNOS) in Raw 264.7 cells plays a important role in promoting the inflammation process through the stimulation of nitric oxide (NO) production (Kanpipit et al., 2022). Moreover, inflammatory molecules were related to collagen degradation caused to human skin aging (Ansary et al., 2021) which is known melatonin can be an antioxidant agent (Skobowiat et al., 2018; Slominski et al., 2014). Thus, melatonin can be anti-aging through reduced reactive oxygen species (ROS)-NO-mediated inflammation and stimulated collagen in dermis skin layers (Kanpipit et al., 2023).

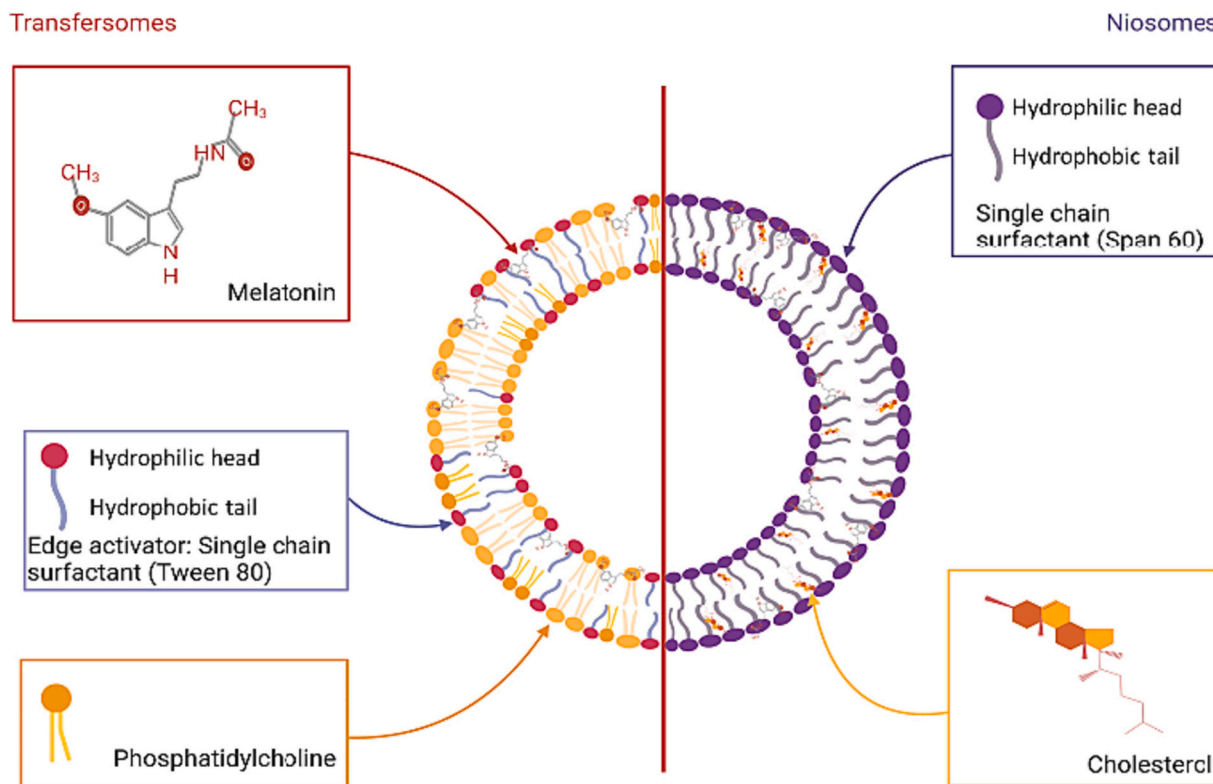*3.1.9.3. Collagen determination.* The evaluation of collagen production

Fig. 5. Structure of transfersomes and niosomes lipid vesicular systems.
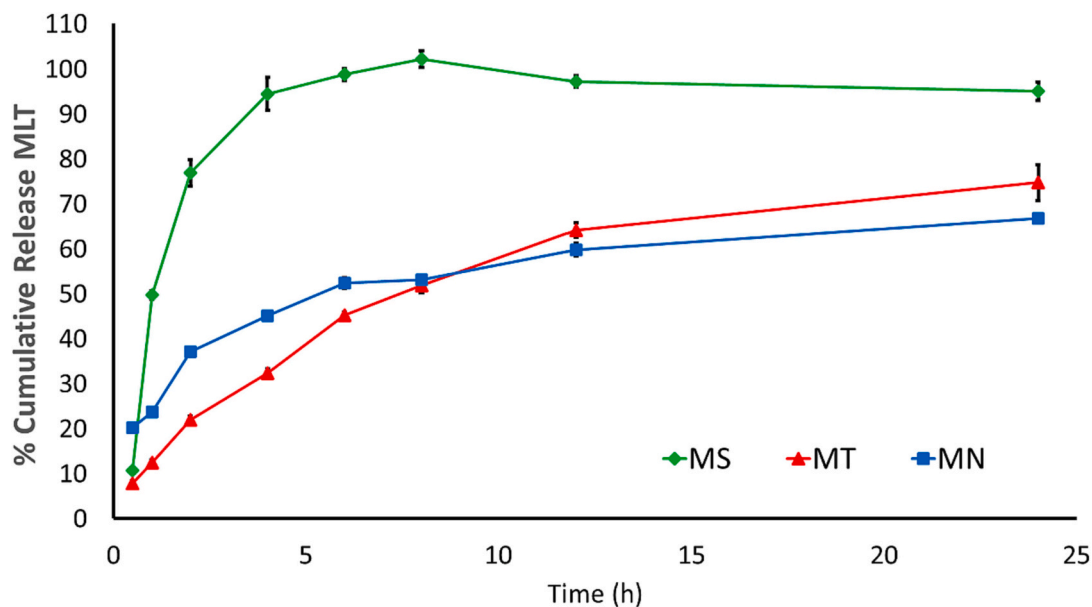

Fig. 6. The release profile of MLT-loaded transfersomes (MT) and MLT-loaded niosomes (MN) compared with MLT solution (MS). The release profile was obtained through cellulose dialysis membrane using Franz diffusion cell for 24 h. All Data presents as mean $\pm$ SEM (n = 3).

in HFF-1 cells was conducted using the picrosirius red method which based on the interaction between the acidic sulfonic groups of the dye and the amino acids presented in collagen (Lareu et al., 2010). Consequently, the dye exhibits a specific affinity to bind with collagen peptides along the entire length of their structure. This in vitro assessment could determine the effectiveness of anti-aging properties. The collagen contents of HFF-1 cells treated by BT, BN, MT, MN, MS and vitamin C were 50.08 ± 0.34, 12.00 ± 1.81, 108.55 ± 2.24, 15.75 ± 1.18, 15.55 ± 1.23 and 112.50 ± 2.74 µg/mL, respectively. Whereas collagen

content of control was 11.01 ± 0.59 µg/mL. The collagen content ratio (sample vs control) is shown in Fig. 9B. The results show that MLT-loaded transfersomes (MT) produced the highest collagen content ratio, which was 9.86-fold of the control as well as the positive control, vitamin C (10.22-fold of control). In addition, BT demonstrated a significantly higher collagen content ratio compared to the control group. While BN, MN, and MS showed increased collagen content compared to the control group, the ratio of collagen content did not exhibit a significant difference when compared to the control group.

Table 2
The release kinetics of MLT-loaded transfersomes (MT) and MLT loaded niosomes (MN) compare MLT solution (MS).

Formulation	Zero order		First order		Higuchi Model		Korsmeyer-Peppas		
	K_0	R^2	K_1	R^2	K_H	R^2	K_p	R^2	n
MT	5.8990	0.9812	0.2332	0.8744	21.1897	0.9955	12.8434	0.9974	0.6870
MN	4.3300	0.8794	0.1249	0.8126	16.0935	0.9551	25.2086	0.9718	0.3766
MS	10.0949	0.7023	0.0899	0.4982	39.1056	0.8287	31.1794	0.7805	0.7143

MT: MLT-loaded transfersomes; MN: MLT-loaded niosomes; MS PEG400: 0.5% MLT in phosphate buffer pH 7.4 with 5% PEG 400; R^2: Coefficient of determination; K_0: Zero order release constant; K_1: First order release constant; K_H: Higuchi release constant; K_p: Korsmeyer-Peppas release constant; n: indicative of the release mechanism.
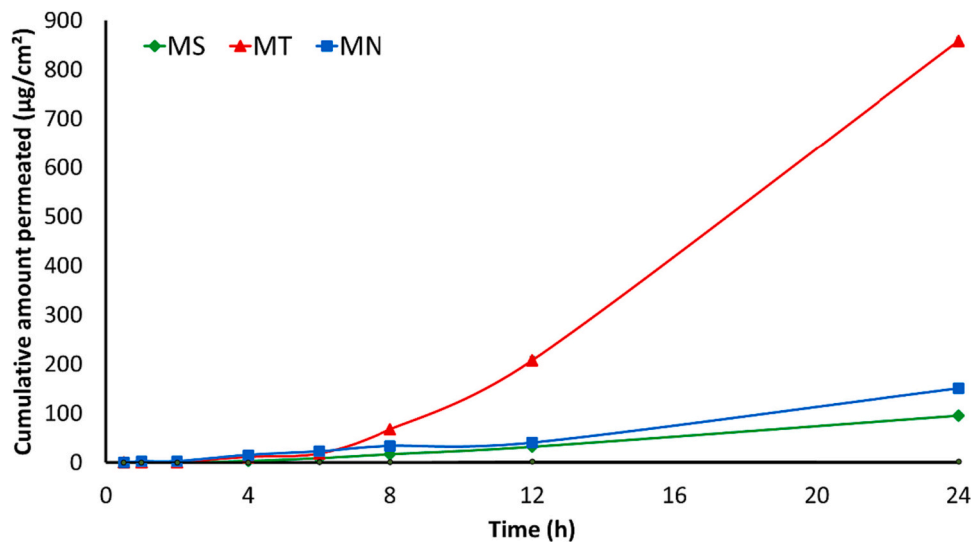

Fig. 7. In vitro permeation of MLT-loaded Transfersomes (MT) and MLT-loaded Niosome (MN) compared with 0.5% MLT solution (MS) through Strat-M® membrane on Franz diffusion cell for 24 h. All the data are presented as mean ± SEM ($n = 3$).

Table 3
Comparison of permeability parameters between MS, MT, and MN. All the values are shown as mean ± SEM ($n = 3$).

Formulation	Flux ($\mu g/cm^2.h$)	$Q24$ ($\mu g/cm^2$)	ER	$Px10^{-3}(cm^2/h)$	$T_{lag}(h)$	Skin deposition($\mu g/cm^2$)
MS	4.66 ± 0.41[a]	94.90 ± 0.87[a]	1	0.93 ± 0.03[a]	4.11 ± 0.06[b]	270.28 ± 4.46[b]
MT	40.74 ± 0.33[c]	858.44 ± 8.08[c]	8.7	8.15 ± 0.07[c]	4.58 ± 0.03[c]	392.47 ± 6.83[c]
MN	6.84 ± 0.11[b]	150.56 ± 1.81[b]	1.5	1.37 ± 0.02[b]	3.13 ± 0.17[a]	214.49 ± 8.90[a]

$Q24$: cumulative amount permeated at 24 h; ER: enhancement ratio; P: permeability coefficient; T_{lag}: Lag time; MS: 0.5% MLT in phosphate buffer pH 7.4 with 5% PEG 400; MT: MLT-loaded transfersomes; MN: MLT-loaded niosomes. [a, b, c] letters indicate difference significance between the group at $p < 0.05$.

Melatonin, known for its antioxidant properties (Skobowiat et al., 2018; Slominski et al., 2014), can potentially exhibit anti-aging effects. It achieves this by reducing reactive oxygen species (ROS)-NO-mediated inflammation and promoting collagen production in the dermal layers of the skin (Kanpipit et al., 2023).

In this study, both MT and MN increased the collagen production in HFF-1 cells. According to a previous study, MLT stimulates the melatonin receptors (MT1 and MT2) located on cell membrane of human skin fibroblasts, thereby enhancing collagen synthesis and providing anti-aging effects. Furthermore, MLT increases the expression of procollagen and decreases the expression of MMP-1. These effects are significant as they contribute to the inhibition of collagen type I and type III synthesis in the dermal layer of the skin (Drobnik et al., 2013).

Moreover, MLT demonstrated a protective capacity in UVA-irradiated primary human dermal fibroblasts by effectively reaching and penetrating intracellular compartments (Koçtürk et al., 2019). In addition, it was found to suppress the expression of UVB-induced MMP-1 and MMP-1 related proteins (inflammatory proteins) and increased procollagen in HaCaT keratinocytes (Park et al., 2018).

4. Conclusions

The incorporation of melatonin into Transfersomes and Niosomes was carried out, and the results revealed several improvements in the physical properties, especially the vesicle size of MLT-loaded transfersome was reduced to approximately 120 nm, and the entrapment efficiency reached 75%. The FTIR determination confirmed the successful incorporation of MLT into the phospholipid bilayer of the transfersomes (MT) demonstrated enhanced sustained release properties, with increased MLT deposition in Strat M® membrane and higher permeation Flux through Strat M® membrane compared to MS and MN. Additionally, MT exhibited improved in vitro efficiency in inhibiting nitric oxide production in RAW 264.7 cells and promoting collagen synthesis in HFF-1 cells, without inducing toxicity. This indicates that MLT-incorporated transfersomes possess significant anti-inflammatory and collagen synthesis properties in vitro. The findings suggest that the developed transfersomes hold potential for applications in the pharmaceutical and cosmeceutical industries. However, further studies, including ex vivo experiments and investigations into other biological activities, are recommended to gain a more comprehensive
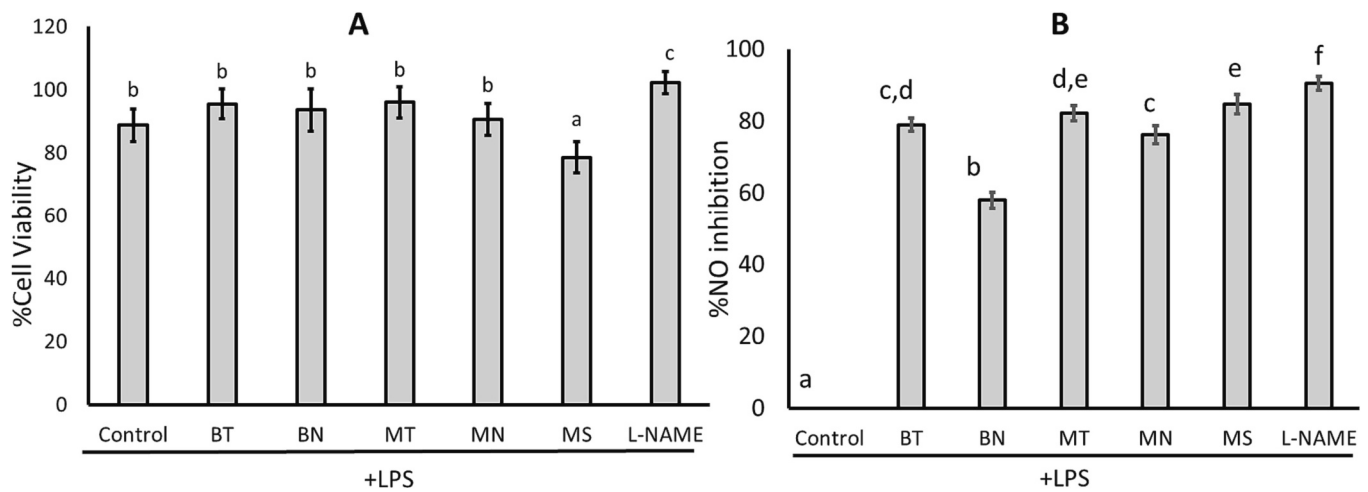
Fig. 8. Cell assay LPS stimulated Raw 264.7 cells (a) Cells viability incubated for 24 h (b): % Nitric oxides inhibition of untreated cells (control), blank transfersomes (BT), blank niosomes (BN), MLT-loaded transfersomes (MT), MLT-loaded niosomes (MN), MLT solution (MS) and positive control (L-NAME, N_{ω}-Nitro-L-arginine methyl ester hydrochloride). [a, b, c, d, e, f, g] letters indicate statistically significant differences between the group at $p < 0.05$. All Data are reported as mean ± SEM ($n = 3$).
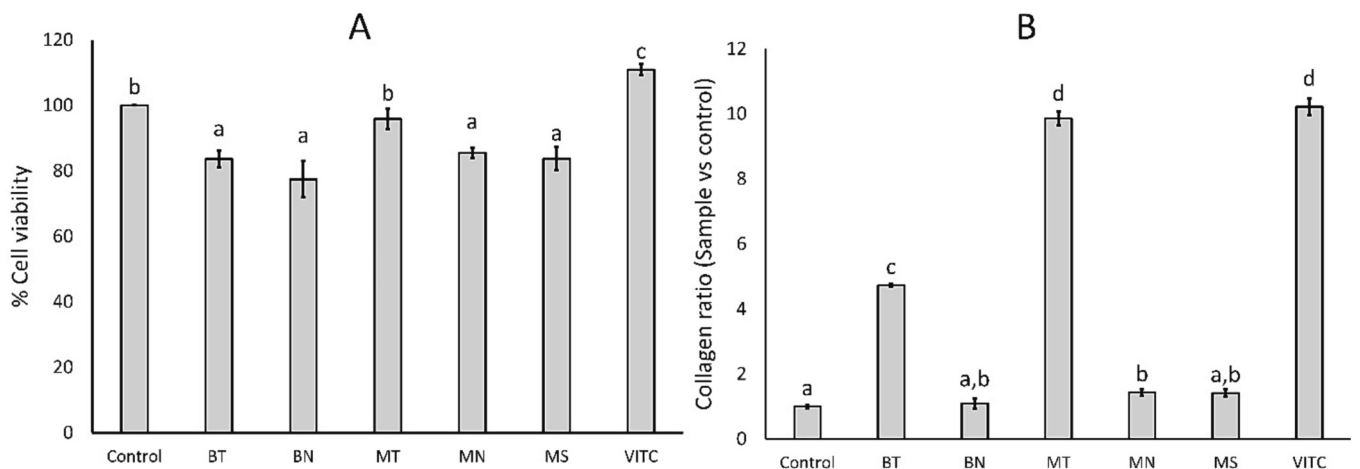
Fig. 9. Cell assay on HFF-1 cells (a): Cell viability after incubated with all samples for 24 h, (b): Collagen ratio (sample vs control) of untreated cells (control), blank transfersomes (BT), blank niosomes (BN), MLT-loaded transfersomes (MT), MLT-loaded niosomes (MN), 0.5%melatonin solution (MS) and vitamin C 50 μg/mL (VITC). [a, b, c, d] letters indicate statistically significant differences between the group at $p < 0.05$. All Data are reported as mean ± SEM ($n = 3$).

understanding of their efficacy.

CRediT authorship contribution statement

Phongsapak Phanphothong: Writing – original draft, Writing – review & editing, Methodology, Data curation, Formal analysis, Visualization, Investigation, Validation. **Nattawadee Kanpipit:** Writing – original draft, Writing – review & editing, Methodology, Data curation, Visualization, Investigation. **Suthasinee Thapphasaraphong:** Supervision, Data curation, Project administration, Conceptualization, Resources, Writing – review & editing.

Declaration of Competing Interest

The authors declare that they have no known competing financial interests or personal relationships that could have appeared to influence the work reported in this paper.

Data availability

No data was used for the research described in the article.

University, Khon Kaen, Thailand, was thanked for facilitating using instruments and equipment. The authors also thank Dr.Glenn Borlace for their English language assistance via the Publication Clinic of Khon Kaen University.

Appendix A. Supplementary data

Supplementary data to this article can be found online at https://doi.org/10.1016/j.ijpx.2023.100217.

References

Agrawal, R., Sandhu, S.K., Sharma, I., Kaur, I.P., 2015. Development and evaluation of curcumin-loaded elastic vesicles as an effective topical anti-inflammatory formulation. AAPS PharmSciTech 16, 364–374. https://doi.org/10.1208/s12249-014-0232-6.

Akbari, J., Saeedi, M., Morteza-Semnani, K., Hashemi, S.M.H., Babaei, A., Eghbali, M., Mohammadi, M., Rostamkalaei, S.S., Asare-Addo, K., Nokhodchi, A., 2022. Innovative topical niosomal gel formulation containing diclofenac sodium (niofenac). J. Drug Target. 30, 108–117. https://doi.org/10.1080/1061186X.2021.1941060.

Al-mahallawi, A.M., Fares, A.R., Abd-Elsalam, W.H., 2019. Enhanced permeation of methotrexate via loading into ultra-permeable niosomal vesicles: Fabrication, statistical optimization, *ex vivo* studies, and *in vivo* skin deposition and tolerability. AAPS PharmSciTech 20, 171. https://doi.org/10.1208/s12249-019-1380-5.

Alvi, I.A., Madan, J., Kaushik, D., Sardana, S., Pandey, R.S., Ali, A., 2011. Comparative study of transfersomes, liposomes, and niosomes for topical delivery of 5-fluorouracil to skin cancer cells: preparation, characterization, in-vitro release, and cytotoxicity analysis. Anti-Cancer Drugs 22, 774–782. https://doi.org/10.1097/CAD.0b013e328346c7d6.

Ameri, M., Lewis, H., Lehman, P., 2018. Effect of skin model on *in vitro* performance of an adhesive dermally applied microarray coated with zolmitriptan. Aust. J. Pharm. 2018, 7459124. https://doi.org/10.1155/2018/7459124.

Ansary, T.M., Hossain, M.R., Kamiya, K., Komine, M., Ohtsuki, M., 2021. Inflammatory molecules associated with ultraviolet radiation-mediated skin aging. Int. J. Mol. Sci. 22, 3974. https://doi.org/10.3390/ijms22083974.

Attia, I.A., El-Gizawy, S.A., Fouda, M.A., Donia, A.M., 2007. Influence of a niosomal formulation on the oral bioavailability of acyclovir in rabbits. AAPS PharmSciTech 8, E106. https://doi.org/10.1208/pt0804106.

Auda, S.H., Fathalla, D., Fetih, G., El-Badry, M., Shakeel, F., 2016. Niosomes as transdermal drug delivery system for celecoxib: *in vitro* and *in vivo* studies. Polym. Bull. 73, 1229–1245. https://doi.org/10.1007/s00289-015-1544-8.

Avadhani, K.S., Manikkath, J., Tiwari, M., Chandrasekhar, M., Godavarthi, A., Vidya, S.M., Hariharapura, R.C., Kalthur, G., Udupa, N., Mutalik, S., 2017. Skin delivery of epigallocatechin-3-gallate (EGCG) and hyaluronic acid loaded nano-transfersomes for antioxidant and anti-aging effects in UV radiation induced skin damage. Drug Deliv. 24, 61–74. https://doi.org/10.1080/10717544.2016.1228718.

Balakrishnan, P., Shanmugam, S., Lee, W.S., Lee, W.M., Kim, J.O., Oh, D.H., Kim, D.-D., Kim, J.S., Yoo, B.K., Choi, H.-G., Woo, J.S., Yong, C.S., 2009. Formulation and *in vitro* assessment of minoxidil niosomes for enhanced skin delivery. Int. J. Pharm. 377, 1–8. https://doi.org/10.1016/j.ijpharm.2009.04.020.

Bansal, S., Aggarwal, G., Chandel, P., Harikumar, S., 2013. Design and development of cefdinir niosomes for oral delivery. J. Pharm. Bioallied Sci. 5, 318. https://doi.org/10.4103/0975-7406.120080.

Bocheva, G., Slominski, R.M., Janjetovic, Z., Kim, T.-K., Böhm, M., Steinbrink, K., Reiter, R.J., Kleszczyński, K., Slominski, A.T., 2022. Protective role of melatonin and its metabolites in skin aging. Int. J. Mol. Sci. 23, 1238. https://doi.org/10.3390/ijms23031238.

Caddeo, C., Manca, M.L., Peris, J.E., Usach, I., Diez-Sales, O., Matos, M., Fernàndez-Busquets, X., Fadda, A.M., Manconi, M., 2018. Tocopherol-loaded transfersomes: in vitro antioxidant activity and efficacy in skin regeneration. Int. J. Pharm. 551, 34–41. https://doi.org/10.1016/j.ijpharm.2018.09.009.

Casanova, F., Santos, L., 2016. Encapsulation of cosmetic active ingredients for topical application–a review. J. Microencapsul. 33, 1–17. https://doi.org/10.3109/02652048.2015.1115900.

Chen, M., Shamim, M.A., Shahid, A., Yeung, S., Andresen, B.T., Wang, J., Nekkanti, V., Meyskens, F.L., Kelly, K.M., Huang, Y., 2020. Topical delivery of carvedilol loaded nano-transfersomes for skin cancer chemoprevention. Pharmaceutics 12, E1151. https://doi.org/10.3390/pharmaceutics12121151.

Chiong, H.S., Yong, Y.K., Ahmad, Z., Sulaiman, M.R., Zakaria, Z.A., Yuen, K.H., Hakim, M.N., 2013. Cytoprotective and enhanced anti-inflammatory activities of liposomal piroxicam formulation in lipopolysaccharide-stimulated RAW 264.7 macrophages. Int. J. Nanomedicine 8, 1245–1255. https://doi.org/10.2147/IJN.S42801.

Dabbagh Moghaddam, F., Akbarzadeh, I., Marzbankia, E., Farid, M., Khaledi, L., Reihani, A.H., Javidfar, M., Mortazavi, P., 2021. Delivery of melittin-loaded niosomes for breast cancer treatment: an *in vitro* and *in vivo* evaluation of anti-cancer effect. Cancer Nanotechnol. 12, 14. https://doi.org/10.1186/s12645-021-00085-9.

De Lima, V.R., Caro, M.S.B., Tavares, M.I.B., Creczynski-Pasa, T.B., 2007. Melatonin location in egg phosphatidylcholine liposomes: possible relation to its antioxidant mechanisms. J. Pineal Res. 43, 276–282. https://doi.org/10.1111/j.1600-079X.2007.00474.x.

Demartis, S., Rassu, G., Murgia, S., Casula, L., Giunchedi, P., Gavini, E., 2021. Improving dermal delivery of rose bengal by deformable lipid nanovesicles for topical treatment of melanoma. Mol. Pharm. 18, 4046–4057. https://doi.org/10.1021/acs.molpharmaceut.1c00468.

Dies, H., Cheung, B., Tang, J., Rheinstädter, M.C., 2015. The organization of melatonin in lipid membranes. Biochim. Biophys. Acta Biomembr. 1848, 1032–1040. https://doi.org/10.1016/j.bbamem.2015.01.006.

Drobnik, J., Owczarek, K., Piera, L., Tosik, D., Olczak, S., Ciosek, J., Hrabec, E., 2013. Melatonin-induced augmentation of collagen deposition in cultures of fibroblasts and myofibroblasts is blocked by luzindole – a melatonin membrane receptors inhibitor. Pharmacol. Rep. 65, 642–649. https://doi.org/10.1016/S1734-1140(13)71041-7.

Dubey, V., Mishra, D., Asthana, A., Jain, N.K., 2006. Transdermal delivery of a pineal hormone: Melatonin via elastic liposomes. Biomaterials 27, 3491–3496. https://doi.org/10.1016/j.biomaterials.2006.01.060.

Dzoyem, J.P., Donfack, A.R.N., Tane, P., McGaw, L.J., Eloff, J.N., 2016. Inhibition of nitric oxide production in LPS-stimulated RAW 264.7 macrophages and 15-LOX activity by anthraquinones from *Pentas schimperi*. Planta Med. 82, 1246–1251. https://doi.org/10.1055/s-0042-104417.

El Zaafarany, G.M., Awad, G.A.S., Holayel, S.M., Mortada, N.D., 2010. Role of edge activators and surface charge in developing ultradeformable vesicles with enhanced skin delivery. Int. J. Pharm. 397, 164–172. https://doi.org/10.1016/j.ijpharm.2010.06.034.

Estanqueiro, M., Conceição, J., Amaral, M.H., Santos, D., Silva, J.B., Lobo, J.M.S., 2014. Characterization and stability studies of emulsion systems containing pumice. Braz. J. Pharm. Sci. 50, 361–369. https://doi.org/10.1590/S1984-82502014000200016.

Farah, H.A., Brown, M.B., McAuley, W.J., 2019. Heat Enhanced Follicular delivery of Isotretinoin to the Skin. Pharm. Res. 36, 124. https://doi.org/10.1007/s11095-019-2659-7.

Farmoudeh, A., Akbari, J., Saeedi, M., Ghasemi, M., Asemi, N., Nokhodchi, A., 2020. Methylene blue-loaded niosome: preparation, physicochemical characterization, and *in vivo* wound healing assessment. Drug Deliv. Transl. Res. 10, 1428–1441. https://doi.org/10.1007/s13346-020-00715-6.

Fernández-García, R., Lalatsa, A., Statts, L., Bolás-Fernández, F., Ballesteros, M.P., Serrano, D.R., 2020. Transferosomes as nanocarriers for drugs across the skin: Quality by design from lab to industrial scale. Int. J. Pharm. 573, 118817 https://doi.org/10.1016/j.ijpharm.2019.118817.

Fitrya, F., Fithri, N.A., Winda, M., Muharni, M., 2022. Ethanol extract of *Parkia speciosa* Hassk. loaded transfersome: Characterization and optimization. J. Pharm. Pharmacogn. Res. 8, 167–176.

Franz, T.J., 1975. Percutaneous absorption on the relevance of *in vitro* data. J. Invest. Dermatol. 64, 190–195. https://doi.org/10.1111/1523-1747.ep12533356.

Gao, Y., Nai, J., Yang, Z., Zhang, J., Ma, S., Zhao, Y., Li, H., Li, J., Yang, Y., Yang, M., Wang, Y., Gong, W., Yu, F., Gao, C., Li, Z., Mei, X., 2021. A novel preparative method for nanoparticle albumin-bound paclitaxel with high drug loading and its evaluation both *in vitro* and *in vivo*. PLoS One 16, e0250670. https://doi.org/10.1371/journal.pone.0250670.

Gupta, P.N., Mishra, V., Rawat, A., Dubey, P., Mahor, S., Jain, S., Chatterji, D.P., Vyas, S.P., 2005. Non-invasive vaccine delivery in transfersomes, niosomes and liposomes: a comparative study. Int. J. Pharm. 293, 73–82. https://doi.org/10.1016/j.ijpharm.2004.12.022.

Haq, A., Michniak-Kohn, B., 2018. Effects of solvents and penetration enhancers on transdermal delivery of thymoquinone: permeability and skin deposition study. Drug Deliv. 25, 1943–1949. https://doi.org/10.1080/10717544.2018.1523256.

Hasibi, F., Nasirpour, A., Varshosaz, J., García-Manrique, P., Blanco-López, M.C., Gutiérrez, G., Matos, M., 2020. Formulation and characterization of taxifolin-loaded lipid nanovesicles liposomes, niosomes, and transfersomes) for beverage fortification. Eur. J. Lipid Sci. Technol. 122, 1900105. https://doi.org/10.1002/ejlt.201900105.

Higuchi, T., 1963. Mechanism of sustained-action medication. Theoretical analysis of rate of release of solid drugs dispersed in solid matrices. J. Pharm. Sci. 52, 1145–1149. https://doi.org/10.1002/jps.2600521210.

Hou, X., Qiu, X., Wang, Y., Song, S., Cong, Y., Hao, J., 2022. Application and efficacy of melatonin elastic liposomes in photoaging mice. Oxidative Med. Cell. Longev. 2022, 1–15. https://doi.org/10.1155/2022/7135125.

Kang, Y.-S., Kang, Y.-G., Park, H.-J., Wee, H.-J., Jang, H.-O., Bae, M.-K., Bae, S.-K., 2013. Melatonin inhibits visfatin-induced inducible nitric oxide synthase expression and nitric oxide production in macrophages. J. Pineal Res. 55, 294–303. https://doi.org/10.1111/jpi.12072.

Kanpipit, N., Nualkaew, N., Kiatponglarp, W., Priprem, A., Thapphasaraphong, S., 2022. Development of a sericin hydrogel to deliver anthocyanins from purple waxy corn cob (*Zea mays* L.) extract and *in vitro* evaluation of anti-Inflammatory effects. Pharmaceutics 14, 577. https://doi.org/10.3390/pharmaceutics14030577.

Kanpipit, N., Nualkaew, N., Thapphasaraphong, S., 2023. The potential of purple waxy corn cob (*Zea mays* L.) extract loaded-sericin hydrogel for anti-hyperpigmentation, UV protection and anti-aging properties as topical product applications. Pharmaceuticals 16, 35. https://doi.org/10.3390/ph16010035.

Kateh Shamshiri, M., Momtazi-Borojeni, A.A., Khodabandeh Shahraky, M., Rahimi, F., 2019. Lecithin soybean phospholipid nano-transfersomes as potential carriers for transdermal delivery of the human growth hormone. J. Cell. Biochem. 120, 9023–9033. https://doi.org/10.1002/jcb.28176.

Khazaeli, P., Pardakhty, A., Shoorabi, H., 2007. Caffeine-loaded niosomes: Characterization and *in vitro* release studies. Drug Deliv. 14, 447–452. https://doi.org/10.1080/10717540701603597.

Kim, A., Lee, E.H., Choi, S.-H., Kim, C.-K., 2004. *In vitro* and *in vivo* transfection efficiency of a novel ultradeformable cationic liposome. Biomaterials 25, 305–313. https://doi.org/10.1016/S0142-9612(03)00534-9.

Kleszczynski, K., Fischer, T.W., 2012. Melatonin and human skin aging. Dermatoendocrinol 4, 245–252. https://doi.org/10.4161/derm.22344.

Koçtürk, S., Yüksel Egrilmez, M., Aktan, Ş., Oktay, G., Resmi, H., Şimşek Keskin, H., Sert Serdar, B., Erkmen, T., Güner Akdogan, G., Özkan, Ş., 2019. Melatonin attenuates the detrimental effects of UVA irradiation in human dermal fibroblasts by suppressing oxidative damage and MAPK/AP-1 signal pathway *in vitro*. Photodermatol. Photoimmunol. Photomed. 35, 221–231. https://doi.org/10.1111/phpp.12456.

Korsmeyer, R.W., Gurny, R., Doelker, E., Buri, P., Peppas, N.A., 1983. Mechanisms of solute release from porous hydrophilic polymers. Int. J. Pharm. 15, 25–35. https://doi.org/10.1016/0378-5173(83)90064-9.

Kumar, G.P., Rajeshwarrao, P., 2011. Nonionic surfactant vesicular systems for effective drug delivery—an overview. Acta Pharm. Sin. B 1, 208–219. https://doi.org/10.1016/j.apsb.2011.09.002.

Kura, A.U., Hussein-Al-Ali, S.H., Hussein, M.Z., Fakurazi, S., 2014. Preparation of tween 80-Zn/Al-levodopa-layered double hydroxides nanocomposite for drug delivery system. Sci. World J. 2014, 1–10. https://doi.org/10.1155/2014/104246.

Kuznetsova, D.A., Vasilieva, E.A., Kuznetsov, D.M., Lenina, O.A., Filippov, S.K., Petrov, K.A., Zakharova, L.Ya., Sinyashin, O.G., 2022. Enhancement of the transdermal delivery of nonsteroidal anti-inflammatory drugs using liposomes containing cationic surfactants. ACS Omega 7, 25741–25750. https://doi.org/10.1021/acsomega.2c03039.

Lareu, R.R., Zeugolis, D.I., Abu-Rub, M., Pandit, A., Raghunath, M., 2010. Essential modification of the Sircol Collagen Assay for the accurate quantification of collagen content in complex protein solutions. Acta Biomater. 6, 3146–3151. https://doi.org/10.1016/j.actbio.2010.02.004.

Longsri, B., Kanpipit, N., Puthongking, P., Mahakunakorn, P., Tiyaworanant, S., Sungthong, B., Thapphasaraphong, S., 2022. Determination of a Chemical Marker in *Dipterocarpus alatus* oleoresin samples and bioactivity screening via antioxidants, nitric oxide Inhibition on murine RAW 264.7 cells, and collagen production on normal human dermal fibroblasts. Trop. J. Nat. Prod. Res. 5, 850–856. https://doi.org/10.26538/tjnpr/v5i5.10.

Mao, W., Wu, F., Lee, R.J., Lu, W., Wang, J., 2019. Development of a stable single-vial liposomal formulation for vincristine. Int. J. Nanomedicine 14, 4461–4474. https://doi.org/10.2147/IJN.S205276.

Marcos, M., Cabaleiro, D., Guimarey, M., Comuñas, M., Fedele, L., Fernández, J., Lugo, L., 2017. PEG 400-based phase change materials nano-enhanced with functionalized graphene nanoplatelets. Nanomaterials 8, 16. https://doi.org/10.3390/nano8010016.

Marwah, H., Garg, T., Rath, G., Goyal, A.K., 2016. Development of transferosomal gel for trans-dermal delivery of insulin using iodine complex. Drug Deliv. 23, 1636–1644. https://doi.org/10.3109/10717544.2016.1155243.

Moroni, I., Garcia-Bennett, A.E., 2021. Effects of absorption kinetics on the catabolism of melatonin released from CAP-coated mesoporous silica drug delivery vehicles. Pharmaceutics 13, 1436. https://doi.org/10.3390/pharmaceutics13091436.

Netweera, V., Limsitthichaikoon, S., Priprem, A., Johns, N.P., 2013. Melatonin encapsulated niosomes permeation characteristics. Int. J. Sci. Adv. Technol. 3, 13–17.

Neupane, R., Boddu, S.H.S., Renukuntla, J., Babu, R.J., Tiwari, A.K., 2020. Alternatives to Biological Skin in Permeation Studies: Current Trends and Possibilities. Pharmaceutics 12, 152. https://doi.org/10.3390/pharmaceutics12020152.

Opatha, S.A.T., Titapiwatanakun, V., Chutoprapat, R., 2020. Transfersomes: a promising nanoencapsulation technique for transdermal drug delivery. Pharmaceutics 12, 855. https://doi.org/10.3390/pharmaceutics12090855.

Panwar, P., Pandey, B., Lakhera, P.C., Singh, K.P., 2010. Preparation, characterization, and in vitro release study of albendazole-encapsulated nanosize liposomes. Int. J. Nanomedicine 5, 101–108. https://doi.org/10.2147/IJN.s8030.

Park, E.K., Lee, H.-J., Lee, H., Kim, J.-H., Hwang, J., Koo, J.I., Kim, S.-H., 2018. The anti-wrinkle mechanism of melatonin in UVB treated HaCaT keratinocytes and hairless mice via Inhibition of ROS and Sonic Hedgehog mediated inflammatory proteins. Int. J. Mol. Sci. 19, 1995. https://doi.org/10.3390/ijms19071995.

Park, S.-E., Yu, H.-Y., Ahn, S., 2021. Development and validation of a simple method to quantify contents of phospholipids in krill oil by fourier-transform infrared spectroscopy. Foods Basel Switz. 11, 41. https://doi.org/10.3390/foods11010041.

Parvez, S., Yadagiri, G., Arora, K., Javaid, A., Kushwaha, A.K., Singh, O.P., Sundar, S., Mudavath, S.L., 2021. Coalition of biological agent (melatonin) with chemotherapeutic agent (amphotericin B) for combating visceral leishmaniasis via oral administration of modified solid lipid nanoparticles. ACS Biomater. Sci. Eng. https://doi.org/10.1021/acsbiomaterials.1c00859.

Phiphatwatcharaded, C., Topark-Ngarm, A., Puthongking, P., Mahakunakorn, P., 2014. Anti-inflammatory activities of melatonin derivatives in lipopolysaccharide-stimulated RAW 264.7 cells and antinociceptive effects in mice. Drug Dev. Res. 75, 235–245. https://doi.org/10.1002/ddr.21177.

Priprem, A., Netweera, V., Mahakunakorn, P., Johns, N.P., Johns, J.R., 2014. Prolonged anti-inflammatory activity of topical melatonin by niosomal encapsulation. Adv. Mater. Res. 902, 70–75. https://doi.org/10.4028/www.scientific.net/AMR.902.70.

Priprem, A., Nukulkit, C., Johns, N.P., Laohasiriwong, S., Yimtae, K., Soontornpas, C., 2018. Transmucosal delivery of melatonin-encapsulated niosomes in a mucoadhesive gel. Ther. Deliv. 9, 343–357. https://doi.org/10.4155/tde-2018-0001.

Rai, S., Pandey, V., Rai, G., 2017. Transfersomes as versatile and flexible nano-vesicular carriers in skin cancer therapy: the state of the art. Nano Rev. Exp. 8, 1325708. https://doi.org/10.1080/20022727.2017.1325708.

Reiter, R.J., Tan, D., Manchester, L.C., Qi, W., 2001. Biochemical reactivity of melatonin with reactive oxygen and nitrogen species: a review of the evidence. Cell Biochem. Biophys. 34, 237–256. https://doi.org/10.1385/CBB:34:2:237.

Sahin, I., Bilge, D., Kazanci, N., Severcan, F., 2013. Concentration-dependent effect of melatonin on DSPC membrane. J. Mol. Struct. 1052, 183–188. https://doi.org/10.1016/j.molstruc.2013.08.060.

Sahu, M., Reddy, V.R.M., Kim, B., Patro, B., Park, C., Kim, W.K., Sharma, P., 2022. Fabrication of Cu_2ZnSnS_4 light absorber using a cost-effective mechanochemical method for photovoltaic applications. Materials 15, 1708. https://doi.org/10.3390/ma15051708.

Sangchart, P., Panyatip, P., Damrongrungruang, T., Priprem, A., Mahakunakorn, P., Puthongking, P., 2021. Anti-inflammatory comparison of melatonin and its bromobenzoylamide derivatives in lipopolysaccharide (LPS)-induced RAW 264.7 cells and croton oil-induced mice ear edema. Molecules 26, 4285. https://doi.org/10.3390/molecules26144285.

Scheuer, C., Pommergaard, H.-C., Rosenberg, J., Gögenur, I., 2014. Melatonin's protective effect against UV radiation: a systematic review of clinical and experimental studies. Photodermatol. Photoimmunol. Photomed. 30, 180–188. https://doi.org/10.1111/phpp.12080.

Shah, P., Goodyear, B., Haq, A., Puri, V., Michniak-Kohn, B., 2020. Evaluations of quality by design (QbD) elements impact for developing niosomes as a promising topical drug delivery platform. Pharmaceutics 12, 246. https://doi.org/10.3390/pharmaceutics12030246.

Skobowiat, C., Brożyna, A.A., Janjetovic, Z., Saowanee, J., Oak, A.S.W., Kim, T.-K., Panich, U., Reiter, R.J., Slominski, A.T., 2018. Melatonin and its derivatives counteract the ultraviolet B radiation-induced damage in human and porcine skin *ex vivo*. J. Pineal Res. 65, e12501 https://doi.org/10.1111/jpi.12501.

Slominski, A.T., Kleszczyński, K., Semak, I., Janjetovic, Z., Żmijewski, M.A., Kim, T.-K., Slominski, R.M., Reiter, R.J., Fischer, T.W., 2014. Local melatoninergic system as the protector of skin integrity. Int. J. Mol. Sci. 15, 17705–17732. https://doi.org/10.3390/ijms151017705.

Taşkiran, D., Taşkiran, E., Yercan, H., Kutay, F.Z., 1999. Quantification of total collagen in rabbit tendon by the sirius red method. Turk. J. Med. Sci. 29, 7–9.

Terakosolphan, W., Trick, J.L., Royall, P.G., Rogers, S.E., Lamberti, O., Lorenz, C.D., Forbes, B., Harvey, R.D., 2018. Glycerol solvates DPPC headgroups and localizes in the interfacial regions of model pulmonary interfaces altering bilayer structure. Langmuir 34, 6941–6954. https://doi.org/10.1021/acs.langmuir.8b00866.

Tewtrakul, S., Itharat, A., 2007. Nitric oxide inhibitory substances from the rhizomes of *Dioscorea membranacea*. J. Ethnopharmacol. 109, 412–416. https://doi.org/10.1016/j.jep.2006.08.009.

Uthaiwat, P., Priprem, A., Puthongking, P., Daduang, J., Nukulkit, C., Chio-Srichan, S., Boonsiri, P., Thapphasaraphong, S., 2021. Characteristic evaluation of gel formulation containing niosomes of melatonin or its derivative and mucoadhesive properties using ATR-FTIR spectroscopy. Polymers 13, 1142. https://doi.org/10.3390/polym13071142.

Wu, P.-S., Li, Y.-S., Kuo, Y.-C., Tsai, S.-J.J., Lin, C.-C., 2019. Preparation and evaluation of novel transfersomes combined with the natural antioxidant resveratrol. Molecules 24, 600. https://doi.org/10.3390/molecules24030600.

Zsikó, S., Cutcher, K., Kovács, A., Budai-Szűcs, M., Gácsi, A., Baki, G., Csányi, E., Berkó, S., 2019. Nanostructured lipid carrier gel for the dermal application of lidocaine: Comparison of skin penetration testing methods. Pharmaceutics 11, 310. https://doi.org/10.3390/pharmaceutics11070310.